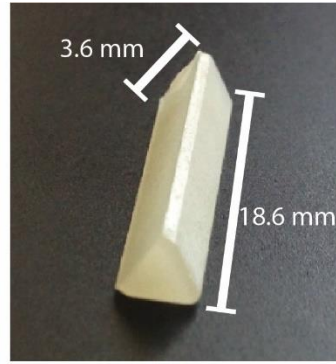
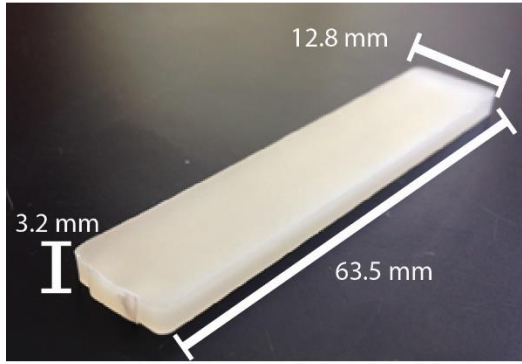


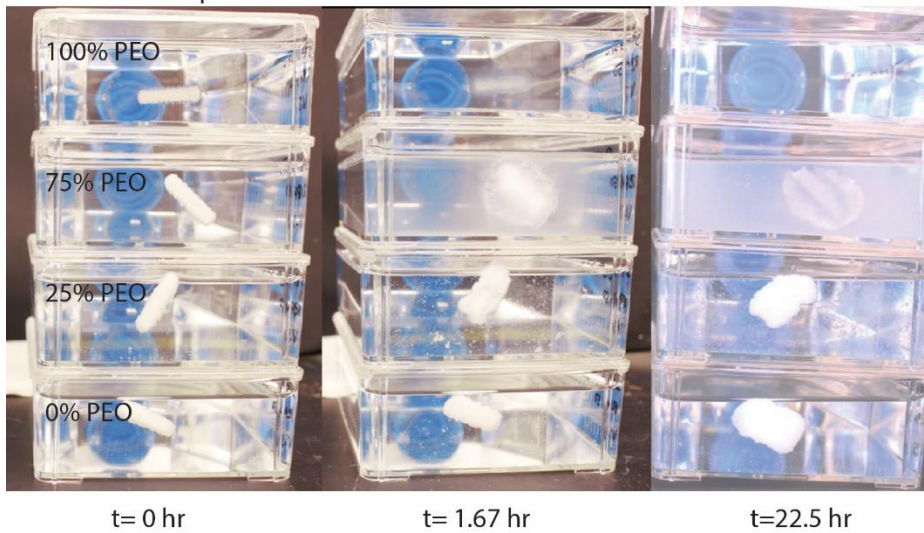
**Supplementary Fig. S1** Contact forces generated by the elastomer core in the LUMI devices. Two of the arms were fixed in an orientation parallel to the bottom surface. The arm of interest was initially held parallel to the bottom surface, and it was instantaneously released. The arm traveled until it collided with the compression platen. The force applied to the compression platen by the arm was measured over time. The picture in the lower right corner shows a LUMI device containing a tempered spring steel and Mediprene core. Plots over time show that the contact force remains constant over time. Bar plots of the data are shown in Figure 2f.



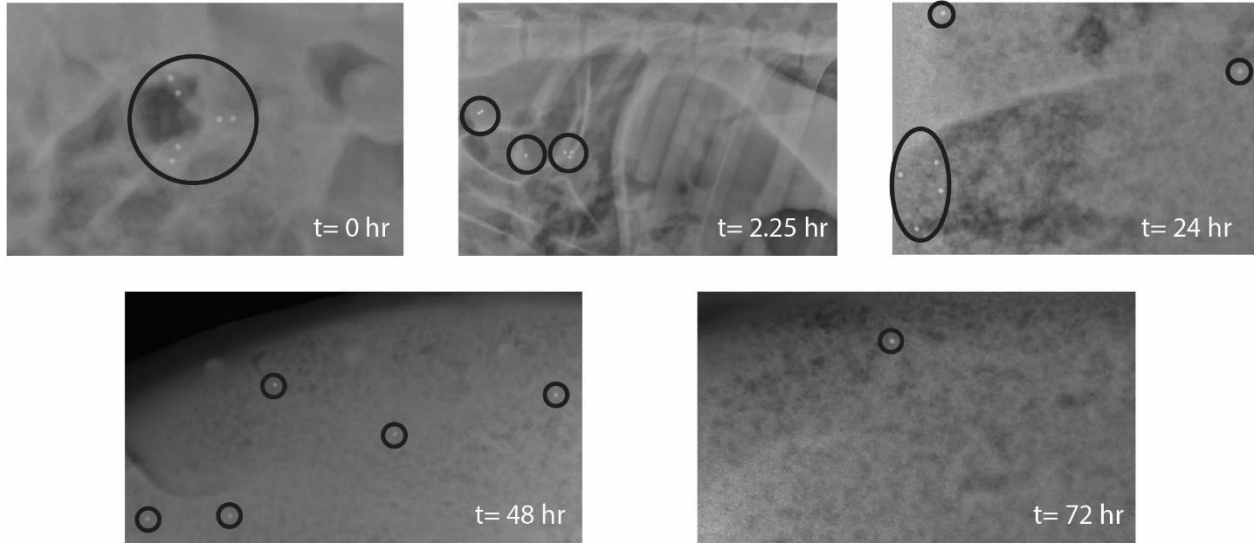
PEO 100k + Soluplus



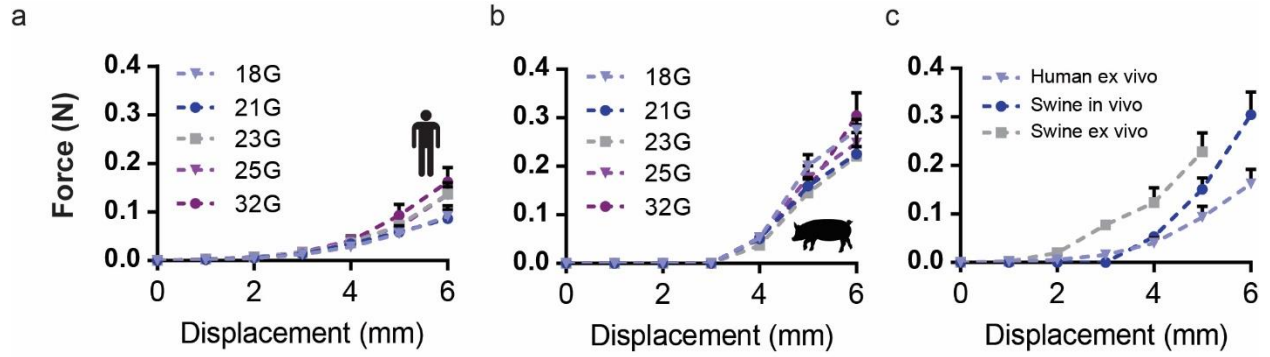
PEO 200k + Soluplus



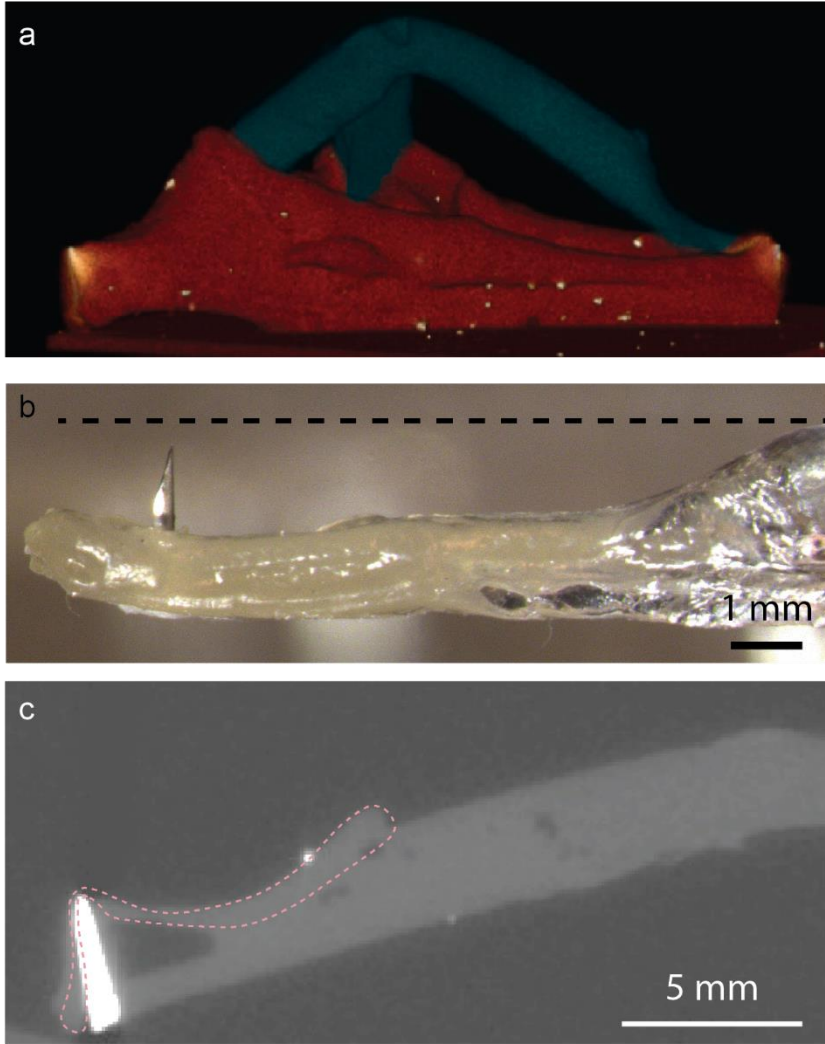
**Supplementary Fig. S2** Bar and arm shape used for dissolution testing. Different PEO and Soluplus<sup>®</sup> mixtures were evaluated for their dissolution timelines.



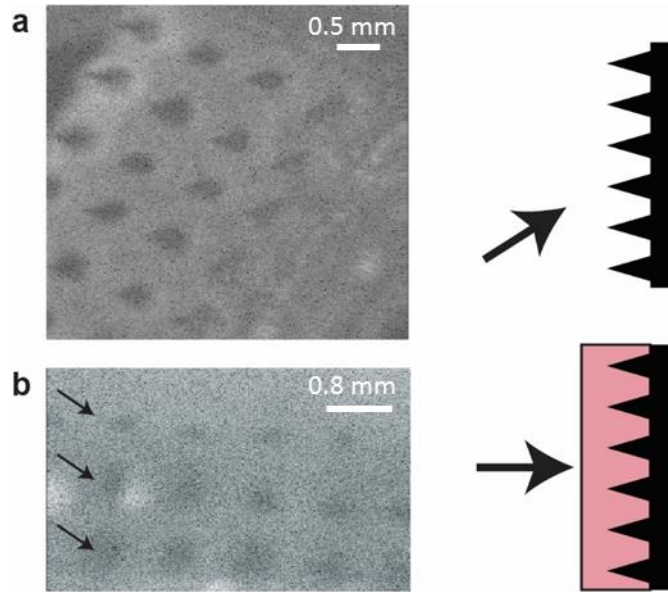
**Supplementary Fig. S3** A LUMI device is delivered to the small intestine in an enteric capsule. Stainless steel ball bearings 1 mm in diameter are placed on the arms to aid in visualization. The device is broken up after 2 hours in the small intestine, and the ball bearings begin to pass out of the GI tract within two days. The metal beads served as radio-opaque fiducials and were not part of the final design.



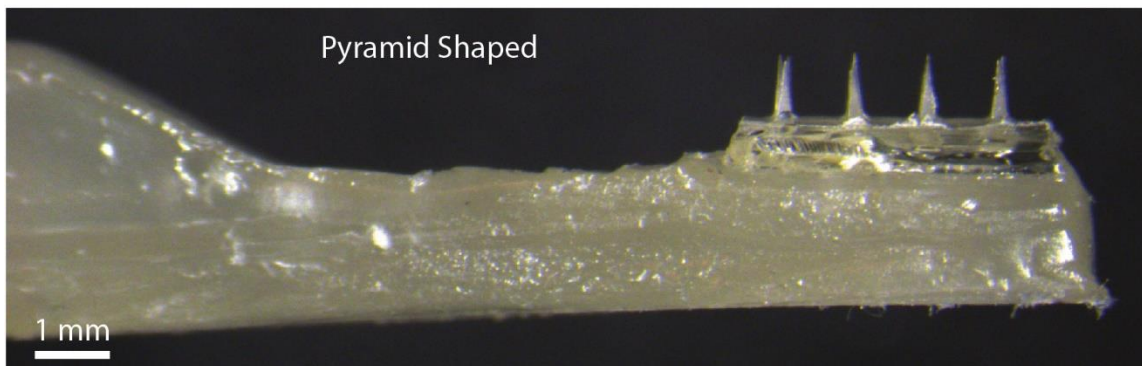
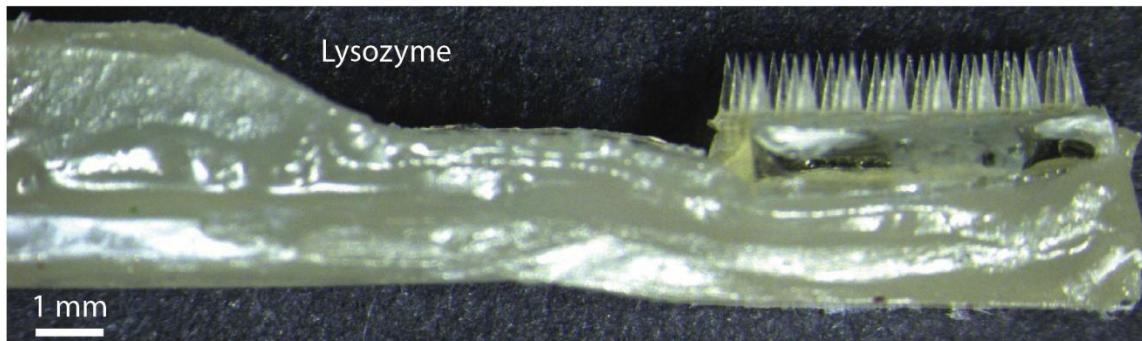
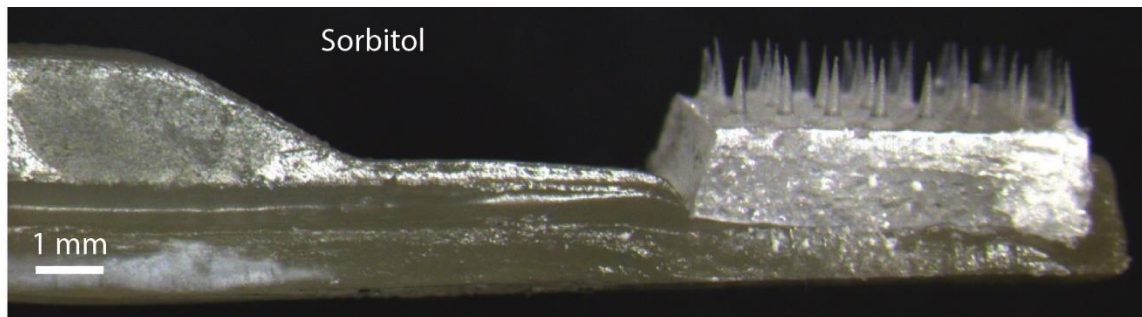
**Supplementary Fig. S4** Penetration characterization for small intestine tissue. Forces required for needle displacement in (a) *ex vivo* human and (b) *in vivo* swine small intestine tissue, respectively. (c) A comparison between human and swine forces in the small intestine using 32 G needles. (Human tissue: n=10 over 3 small intestines; swine tissue (in vivo and ex vivo): n=15 over 3 small intestines. Error bars=SD.)



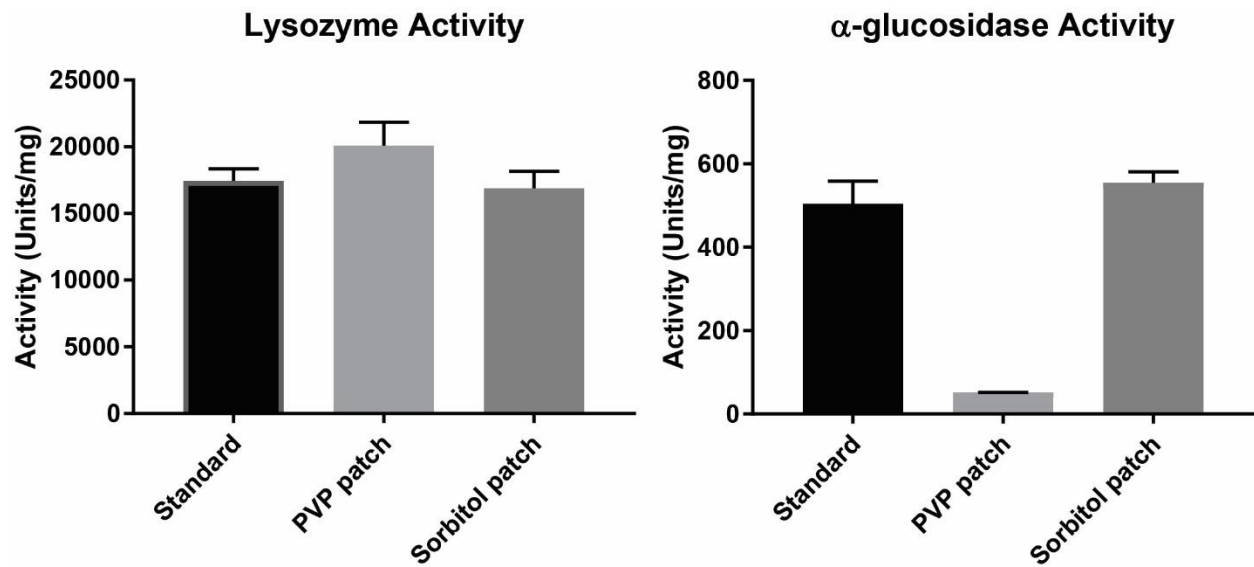
**Supplementary Fig. S5** LUMI deployment with hypodermic needle. (a) Colored MicroCT reconstruction. (b) Needle is same height as microneedles. (c) MicroCT of LUMI deployment. Tissue is outlined in pink.



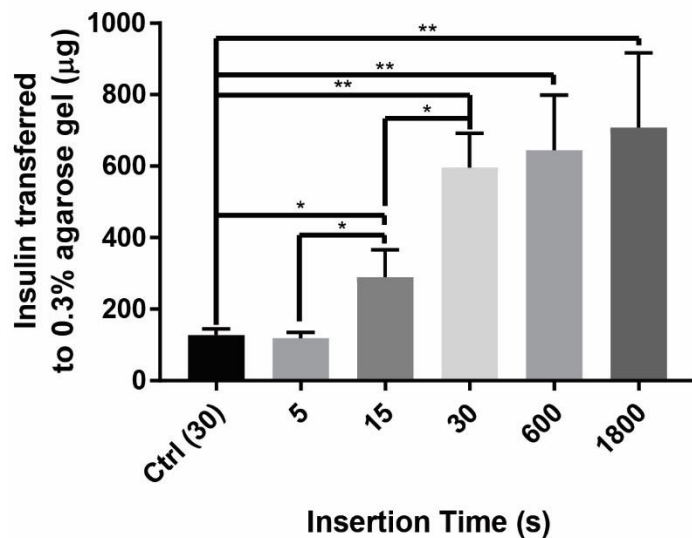
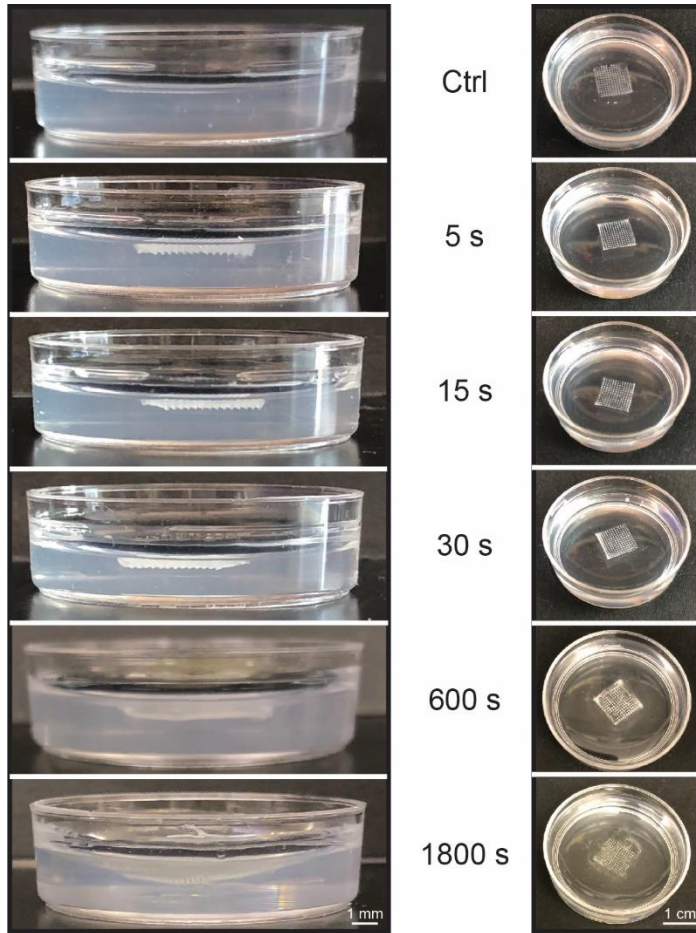
**Supplementary Fig. S6** Optical coherence tomography (OCT) images showing the microneedles mounted in the LUMI arm (a) prior to insertion and (b) inserted into small intestine after deploying the arm from a 30 degree angle. Arrows in figure b point to the holes observed in the tissue corresponding to microneedles being inserted. The differences in the holes' size reflect the different penetration depths from tilted insertion. Animations to the right denote the angle of the imager compared to the microneedle patch on the LUMI arm.



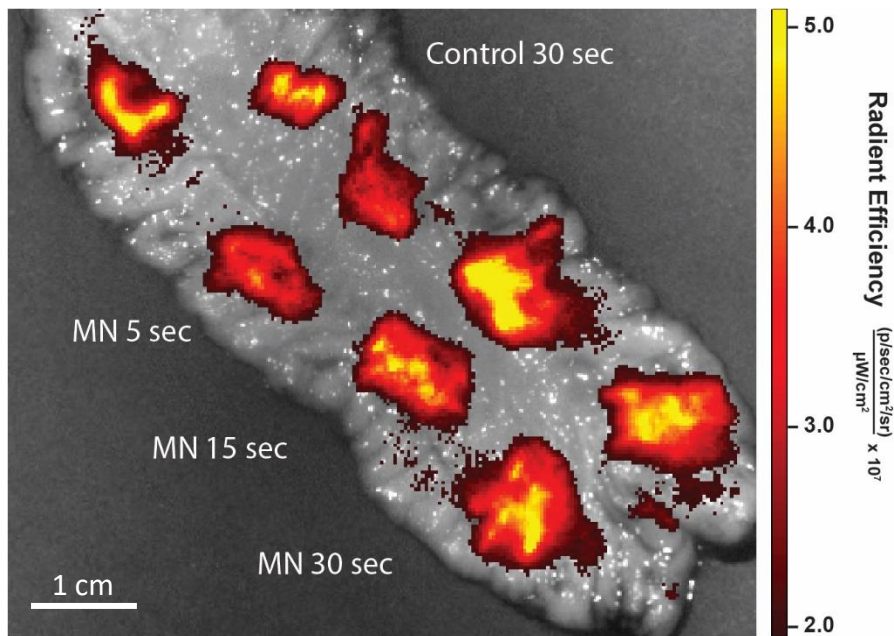
**Supplementary Fig. S7** LUMI arms with microneedle patches made with different formulations and active pharmaceutical ingredients. Aside from the sorbitol patch, all patches use polyvinylpyrrolidone as a binding agent.



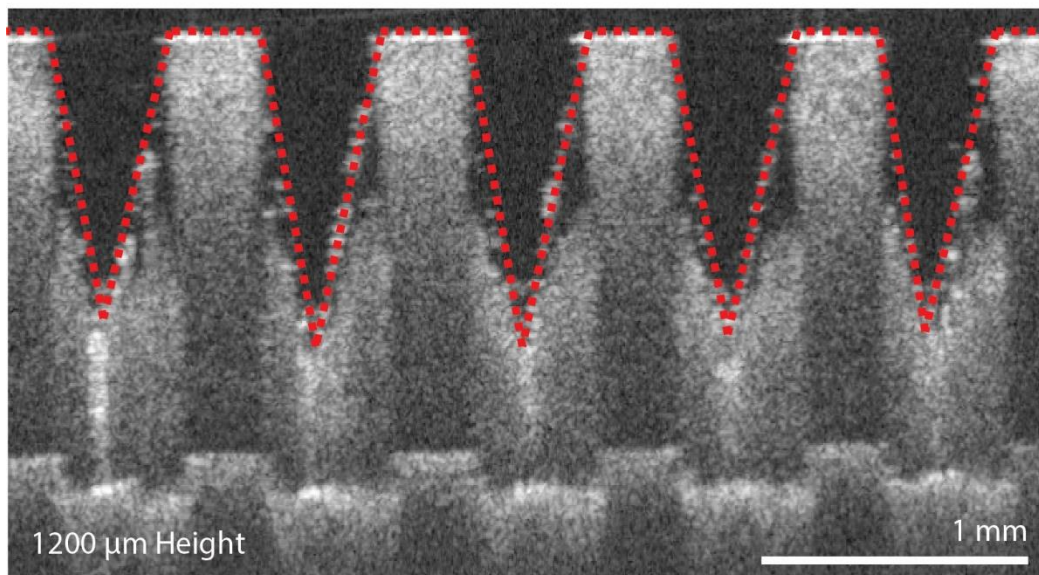
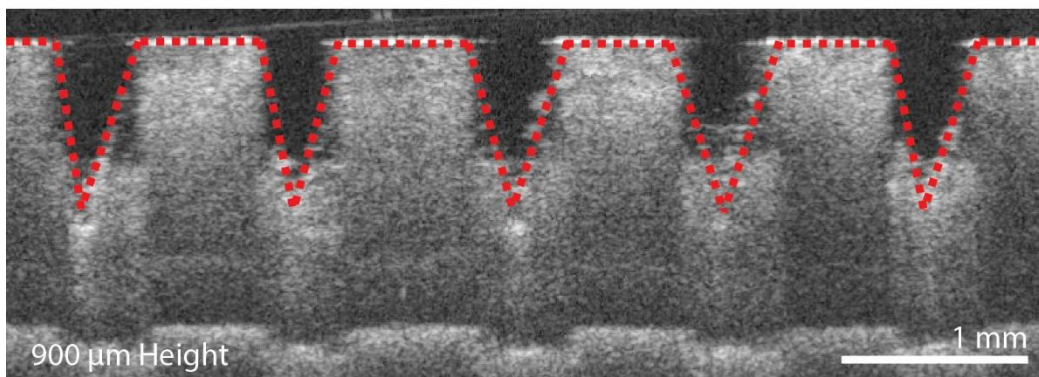
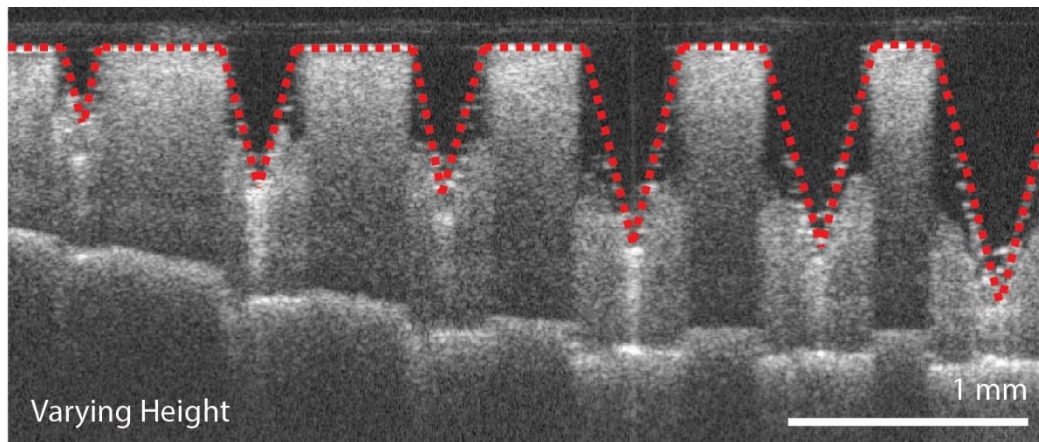
**Supplementary Fig. S8** Activity of lysozyme and alpha-glucosidase in microneedle formulations. PVP = Polyvinylpyrrolidone. (n=3. Error Bars=SD)



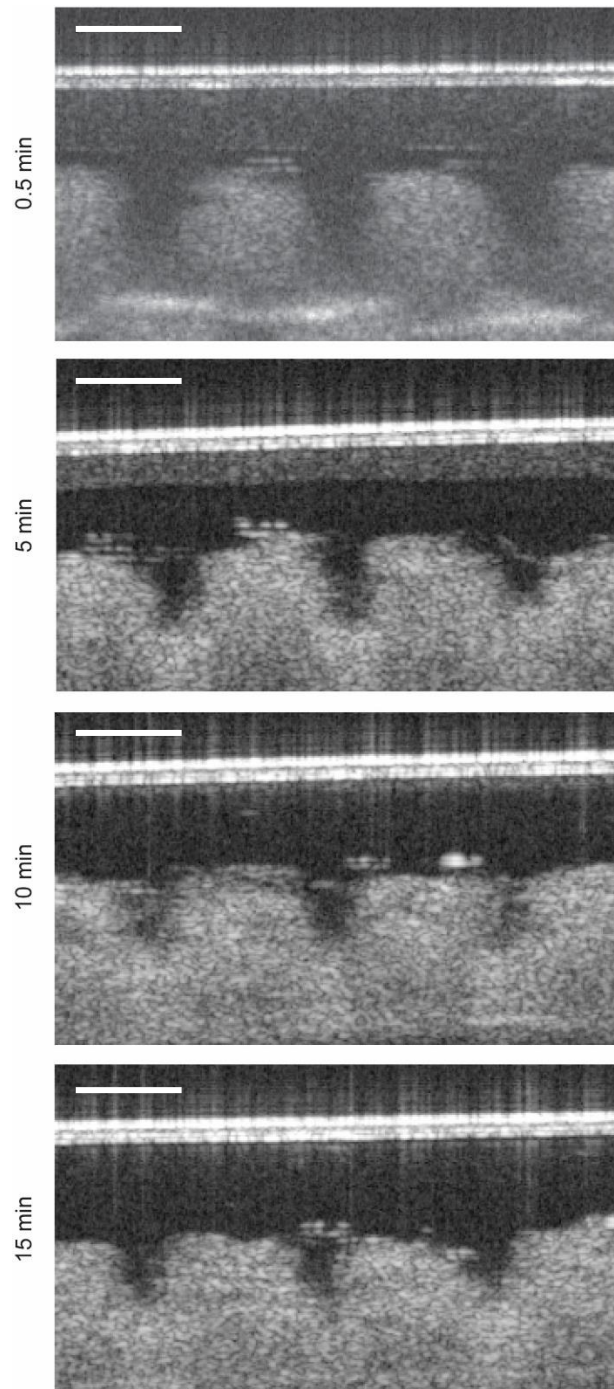
**Supplementary Fig. S9** Insulin microneedle patch dissolution in 0.3% agarose gel. Patches which were inserted into the gel for a set period of time were compared to patches which were laid on top of the gel for 30 seconds (control). The figure also includes views of the gel from the side (left) and top (right) after the patch was removed. The insulin transferred from the patch to the gel was quantified via HPLC. (n=3. Error Bars=SD; \*P<0.05, \*\*P<0.01).



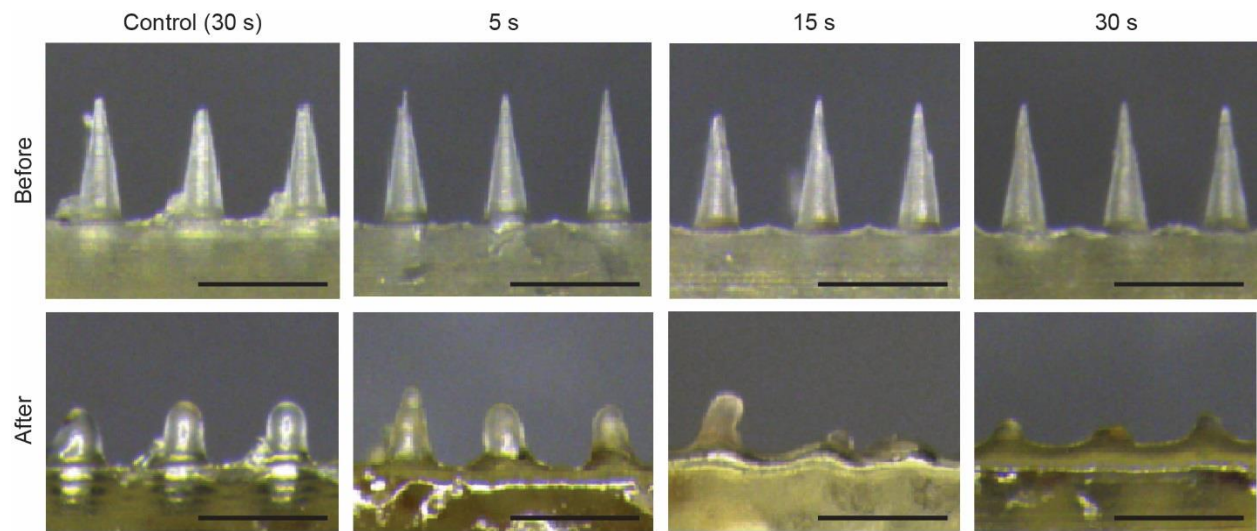
**Supplementary Fig. S10** In vivo imaging system image of swine tissue applied with Texas red loaded microneedle patches. Patches were applied *in vivo*. The tissue was harvested and imaged within 3 hours. Each set of patches were applied for varying amounts of time. The control patches were left to sit on top of the tissue, but they were not pressed into the tissue.



**Supplementary Fig. S11** OCT images of microneedles of varying lengths inserted into swine small intestine tissue. Lighter gray represents small intestine tissue. Discontinuous vertical shifts result from the varying optical path lengths from different refractive index materials.



**Supplementary Fig. S12** OCT imaging showing dissolution of microneedle patches in *ex vivo* swine tissue. The space that the microneedle creates within the swine tissue gradually decreases as a function of time (scale bars a 0.5 mm).



**Supplementary Fig. S13** Dissolution of insulin microneedle patches applied to *in vivo* swine small intestine. Control patches were laid upon the tissue and all other patches were penetrated into to the tissue (scale bars are 1 mm).



**Supplementary Fig. S14** LUMI fabrication process. Custom fabricated PDMS mold for creation of LUMI backbone. We used Mediprene for the elastomer core and a PEO/Soluplus<sup>®</sup> mixture for the arms. Metal cores were embedded in the elastomer during heating.



**Supplementary Fig. S15** Fixture used to release LUMI *ex vivo* for OCT imaging. The tissue was fixed to the top section of the fixture using push pins. Two LUMI arms were fixed using the LUMI holder and another arm was placed underneath the wire (marked with yellow tape). The LUMI holder was then placed under the tissue fixture. The arm was then released and allowed to unfold after removing the wire.

	Age	Sex	Race	Height (in)	Weight (lbs)	Mode of Death
Patient 1	45	F	C	62	120	Multiple sclerosis
Patient 2	70	F	C	63	97	Respiratory Failure
Patient 3	32	F	C	67	176	Anoxia

**Supplementary Table S1:** Human Patient data from small intestine penetration study. Characteristics of the patients from which the stomachs were acquired.